NASA/TM—2019–220363

TESS Data Release Notes:
Sector 14, DR19

Michael M. Fausnaugh, Christopher J. Burke
Kavli Institute for Astrophysics and Space Science, Massachusetts Institute of Technology, Cambridge, Massachusetts

Douglas A. Caldwell
SETI Institute, Mountain View, California

Jon M. Jenkins
NASA Ames Research Center, Moffett Field, California

Jeffrey C. Smith, Joseph D. Twicken
SETI Institute, Mountain View, California

Roland Vanderspek
Kavli Institute for Astrophysics and Space Science, Massachusetts Institute of Technology, Cambridge, Massachusetts

John P. Doty
Noqsi Aerospace Ltd, Billerica, Massachusetts

Eric B. Ting
Ames Research Center, Moffett Field, California

Joel S. Villasenor
Kavli Institute for Astrophysics and Space Science, Massachusetts Institute of Technology, Cambridge, Massachusetts

September 19, 2019

Acknowledgements

These Data Release Notes provide information on the processing and export of data from the Transiting Exoplanet Survey Satellite (TESS). The data products included in this data release are full frame images (FFIs), target pixel files, light curve files, collateral pixel files, cotrending basis vectors (CBVs), and Data Validation (DV) reports, time series, and associated xml files.

These data products were generated by the TESS Science Processing Operations Center (SPOC, Jenkins et al., 2016) at NASA Ames Research Center from data collected by the TESS instrument, which is managed by the TESS Payload Operations Center (POC) at Massachusetts Institute of Technology (MIT). The format and content of these data products are documented in the Science Data Products Description Document (SDPDD)[1]. The SPOC science algorithms are based heavily on those of the Kepler Mission science pipeline, and are described in the Kepler Data Processing Handbook (Jenkins, 2017).[2] The Data Validation algorithms are documented in Twicken et al. (2018) and Li et al. (2019). The TESS Instrument Handbook (Vanderspek et al., 2018) contains more information about the TESS instrument design, detector layout, data properties, and mission operations.

The TESS Mission is funded by NASA's Science Mission Directorate.

This report is available in electronic form at
https://archive.stsci.edu/tess/

[1]https://archive.stsci.edu/missions/tess/doc/EXP-TESS-ARC-ICD-TM-0014.pdf

[2]https://archive.stsci.edu/kepler/manuals/KSCI-19081-002-KDPH.pdf

1 Observations

TESS Sector 14 observations include physical orbits 35 and 36 of the spacecraft around the Earth. Data collection was paused for 0.95 days during perigee passage while downloading data. In total, there are 25.91 days of science data collected in Sector 14.

Table 1: Sector 14 Observation times

	UTC	TJD[a]	Cadence #
Orbit 35 start	2019-07-18 20:19:29	1683.34838	328243
Orbit 35 end	2019-07-31 21:17:29	1696.38865	337632
Orbit 36 start	2019-08-01 20:05:29	1697.33865	338316
Orbit 36 end	2019-08-14 16:51:28	1710.20392	347579

[a] TJD = TESS JD = JD - 2,457,000.0

The spacecraft was pointing at RA (J2000): 276.7169°; Dec (J2000): 62.4756°; Roll: 32.2329°. Two-minute cadence data were collected for 20,000 targets, and full frame images were collected every 30 minutes. See the TESS project Sector 14 observation page[3] for the coordinates of the spacecraft pointing and center field-of-view of each camera, as well as the detailed target list. Fields-of-view for each camera and the Guest Investigator two-minute target list can be found at the TESS Guest Investigator Office observations status page[4].

A number of important changes were made in Sector 14, which are described in detail below. For ease of reference, here is a brief summary:

- Sector 14 is the first northern ecliptic hemisphere pointing.
- Sector 14 is the first sector to make use of TIC 8, which is based on Gaia DR2 astrometry and photometry, and uses Gaia DR2 parallaxes to inform stellar parameters. Full details are provided by Stassun et al. (2019) and the TIC release notes[5].
- In Sector 14, the spacecraft is pointed to a higher ecliptic latitude (+85 degrees rather than +54 degrees) to mitigate issues with scattered light in Camera 1 and Camera 2—see §1.3.
- Sector 14 processing is the first to make use of an updated SPOC data processing pipeline, SPOC Release 4.0 —see §4.2 for details.
- Sector 14 is the first to make use of CCD-specific Data Anomaly Flags that mark cadences excluded due to high levels of scattered light. The flags are referred to as "Scattered Light" flags and marked with bit 13, value 4096—see §2 for more details.

[3] https://tess.mit.edu/observations/sector-14
[4] https://heasarc.gsfc.nasa.gov/docs/tess/status.html
[5] https://outerspace.stsci.edu/display/TESS/TIC+v8+and+CTL+v8.xx+Data+Release+Notes

1.1 Notes on Individual Targets

Seven very bright stars (Tmag $\lesssim$ 1.8) with large pixel stamps were not processed in the photometric pipeline. Target pixel files with raw data are provided, but no light curves were produced. The affected TIC IDs are 471012017, 157587146, 99843265, 229540730, 329269366, 164642404, and 237195876.

Five target stars (1715683214, 1715683215, 441804565, 471012056, and 471012067) are blended with bright stars—the contaminating flux for these objects is very large, and the resulting photometry for such targets is expected to be unreliable.

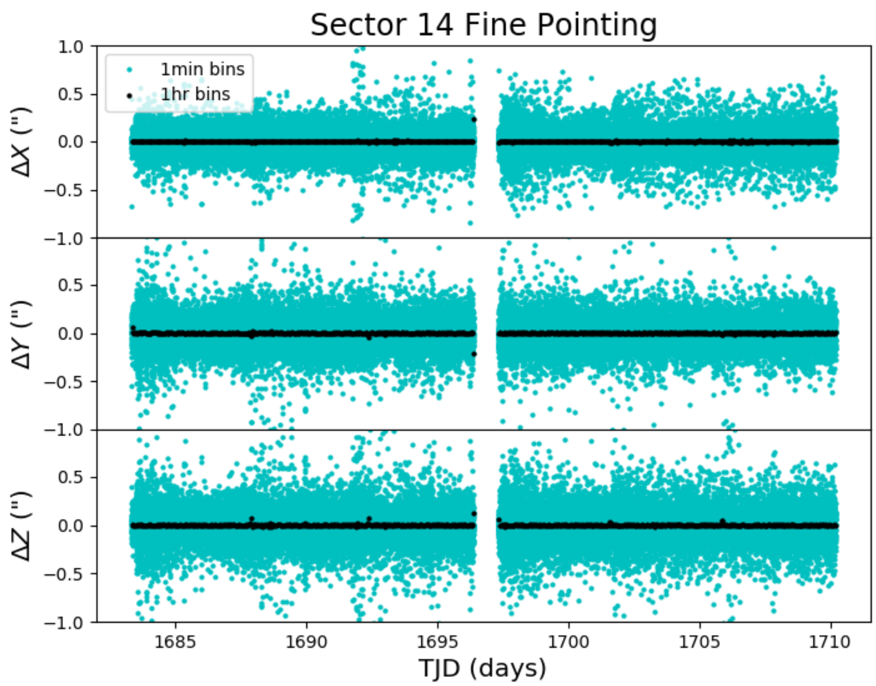

Figure 1: Guiding corrections based on spacecraft fine pointing telemetry. The delta-quaternions from each camera have been converted to spacecraft frame, binned to 1 minute and 1 hour, and averaged across cameras. Long-term trends (such as those caused by differential velocity aberration) have also been removed. The ΔX/ΔY directions represent offsets along the the detectors' rows/columns, while the ΔZ direction represents spacecraft roll.

1.2 Spacecraft Pointing and Momentum dumps

Sector 14 is the first sector of the northern ecliptic hemisphere survey. For northern pointings, scattered light from the Earth and Moon is a more persistent issue for Camera 1 and Camera 2 than for southern pointings. For this reason, the spacecraft pointing was set at +85 degrees in ecliptic latitude, so that Camera 2 and Camera 3 straddle the ecliptic pole. Camera 1 still suffers from strong scattered light signals (see §1.3), and so guiding was disabled in Camera 1 for both orbits 35 and 36. Camera 4 alone was used for guiding in all of orbits 35 and 36.

The reaction wheel speeds were reset with momentum dumps every 4.4 days. Figure 1 summarizes the pointing performance over the course of the sector based on Fine Pointing telemetry.

1.3 Scattered Light

Figure 2 shows the median value of the background estimate for all targets on a given CCD as a function of time. Figure 3 shows the angle between each camera's boresight and the Earth or Moon—this figure can be used to identify periods affected by scattered light and the relative contributions of the Earth and Moon to the image backgrounds.

In Sector 14, the Earth is above the sunshade for almost the entire sector, and the backgrounds are somewhat higher for longer periods of time than in other sectors. The 24 hour rotation period of the Earth and several harmonics thereof are also visible as oscillations in the background for most of both orbits. Finally, the Earth passes close to Camera 1 towards the last quarter of each orbit and saturates the detectors—these times were excluded with CCD-specific "Scattered Light" flags (see §2).

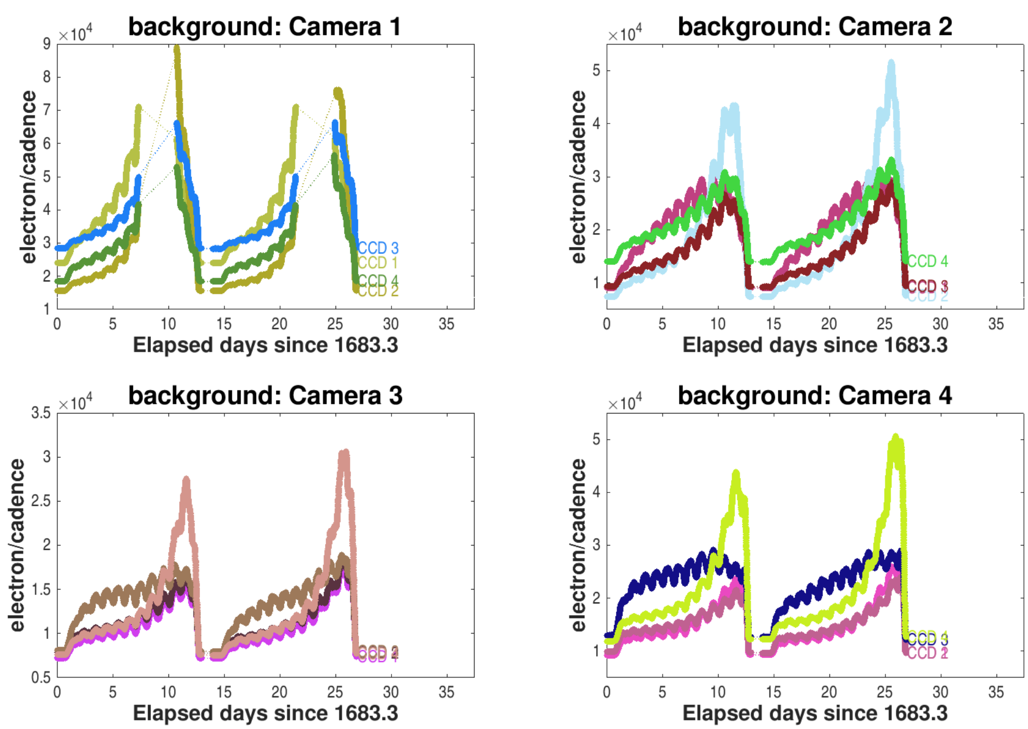

Figure 2: Median background flux across all targets on a given CCD in each camera. The changes are caused by variations in the orientation and distance of the Earth and Moon.

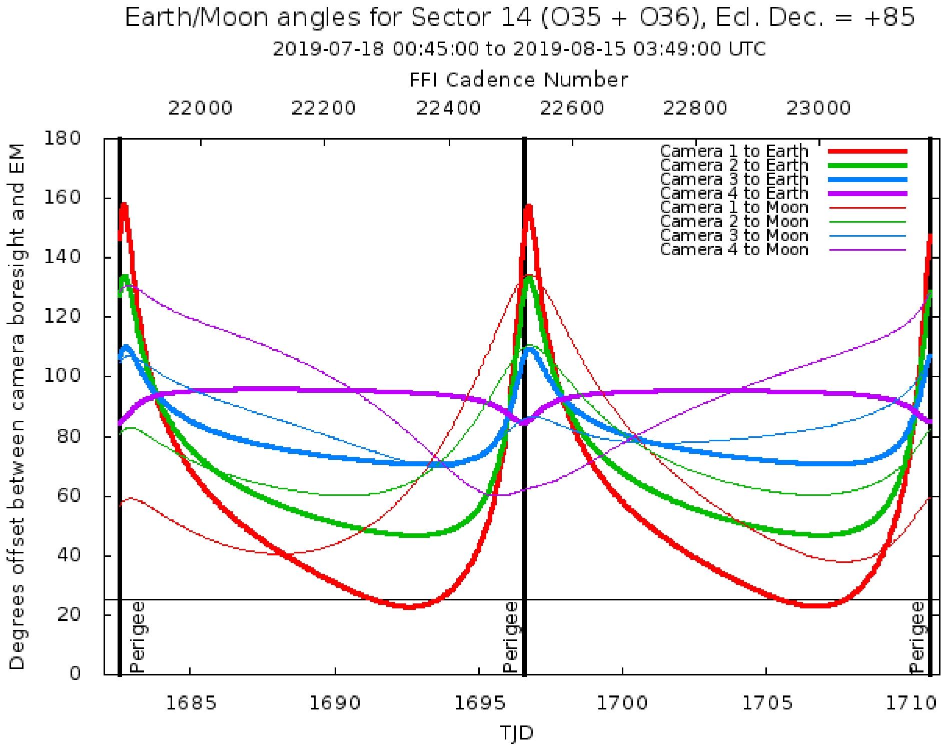

Figure 3: Angle between the four camera boresights and the Earth/Moon as a function of time. When the Earth is within $\sim 25°$ of a camera's boresight, transiting planet searches may be compromised by high levels of scattered light. At larger angles, up to $\sim 35°$, scattered light patterns and complicated structures may be visible. At yet larger angles, low level patchy features may be visible. Scattered light from the Moon is generally only noticeable below $\sim 35°$. This figure can be used to identify periods affected by scattered light and the relative contributions of the Earth and Moon to the background. However, the background intensity and locations of scattered light features depend on additional factors, such as the Earth/Moon azimuth and distance from the spacecraft.

2 Data Anomaly Flags

See the SDPDD (§9) for a list of data quality flags and the associated binary values used for TESS data, and the TESS Instrument Handbook for a more detailed description of each flag. Note that a new Data Anomaly flag has been added for the two-minute target data in Sector 14.

The following flags were not used in Sector 14: bits 1, 2, 7, 9, and 11 (Attitude Tweak, Safe Mode, Cosmic Ray in Aperture, Discontinuity, Cosmic Ray in Collateral Pixel).

Cadences marked with bits 3, 4, 6, and 12 (Coarse Point, Earth Point, Reaction Wheel Desaturation Event, and Straylight) were marked based on spacecraft telemetry.

Cadences marked with bit 5 and 10 (Argabrightening Events and Impulsive Outlier) were identified by the SPOC pipeline. Bit 5 marks a sudden change in the background measurements. In practice, bit 5 flags are caused by rapidly changing glints and unstable pointing at times near momentum dumps. Bit 10 marks an outlier identified by PDC and omitted from the cotrending procedure.

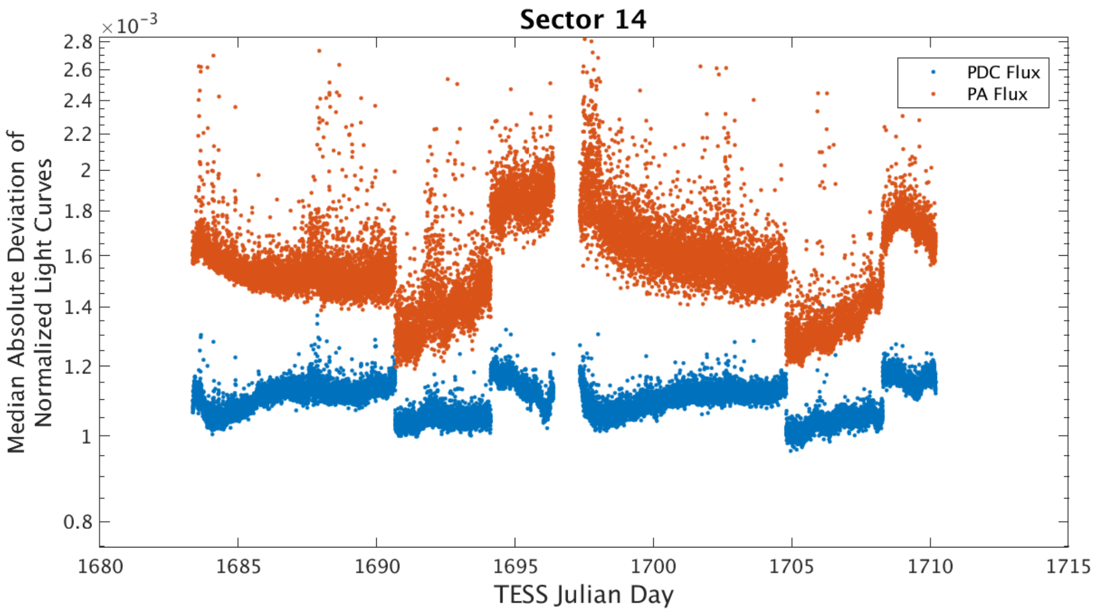

Figure 4: Median absolute deviation (MAD) for the 2-minute cadence data from Sector 14, showing the performance of the cotrending after identifying Manual Exclude data quality flags. The MAD is calculated in each cadence across stars with flux variations less than 1% for both the PA (red) and PDC (blue) light curves, where each light curve is normalized by its median flux value. The scatter in the PA light curves is much higher than that for the PDC light curves, and the outliers in the PA light curves are largely absent from the PDC light curves due to the use of the anomaly flags.

Cadences marked with bit 8 (Manual Exclude) are ignored by PDC, TPS, and DV for cotrending and transit searches. In Sector 14, these cadences were identified using spacecraft telemetry from the fine pointing system. All cadences with pointing excursions >21 arcseconds (∼1 pixel) were flagged for manual exclude. See Figure 4 for an assessment of the performance of the cotrending based on the final set of manual excludes. The dip regions beginning at TJD ∼1690 and ∼1705 are due to the new scattered light flags on Camera 1.

In Sector 14, a new Data Anomaly Flag represented by bit 13 (value 4096, "Scattered Light") has been introduced to mark cadences during times of strong scattered light signals. These cadences would negatively affect the systematic error removal in PDC and the planet search in TPS and are excluded from the pipeline analysis. The cadences are selected by identifying times when the background measurements rise above a given threshold on each CCD. "Scattered Light" flags are therefore only applied to targets on specific CCDs, and the cadences marked with this flag are different for each CCD. Raw and flux-calibrated (without background correction) pixels are provided in the target pixel files for these cadences, but no photometry or centroid positions are calculated. These data anomaly flags replace the procedure for gapped cadence ranges reported in Table 2 of Data Releases 11, 14, 16, 17, and 18 (Sectors 9, 10, 11, 12, and 13, respectively).

FFIs were only marked with bits 3, 6 and 12 (Course Point, Reaction Wheel Desaturation Events and Straylight). Only one FFI is affected by each momentum dump.

3 Anomalous Effects

3.1 Smear Correction Issues

The following column was impacted by bright stars in the upper buffer rows, which bleed into the upper serial register resulting in an overestimated smear correction.

- Camera 3, CCD 1, Column 281, Star HD 106381
- Camera 4, CCD 4, Column 1181, Star HD 145603

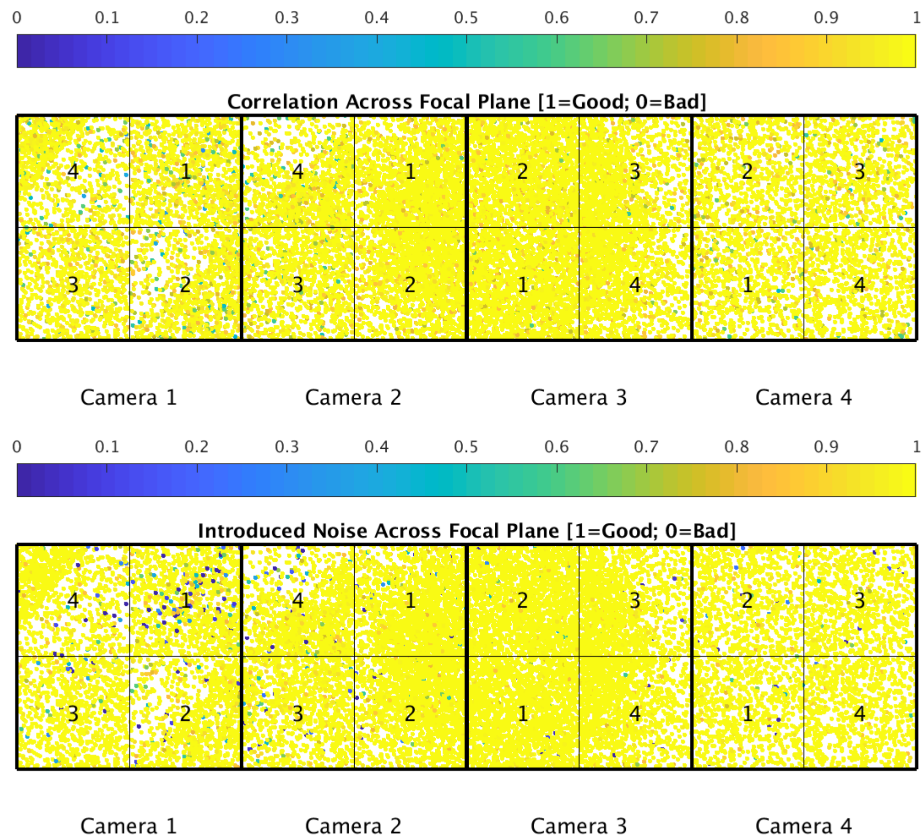

Figure 5: PDC residual correlation goodness metric (top panel) and PDC introduced noise goodness metric (bottom panel). The metric values are shown on a focal plane map indicating the camera and CCD location of each target. The correlation goodness metric is calibrated such that a value greater than 0.8 means there is less than 10% mean absolute correlation between the target under study and all other targets on the CCD. The introduced noise metric is calibrated such that a value greater than 0.8 means the power in broad-band introduced noise is below the level of uncertainties in the flux values.

3.2 Fireflies and Fireworks

Table 2 lists all firefly and fireworks events for Sector 14. These phenomena are small, spatially extended, comet-like features in the images—created by sunlit particles in the

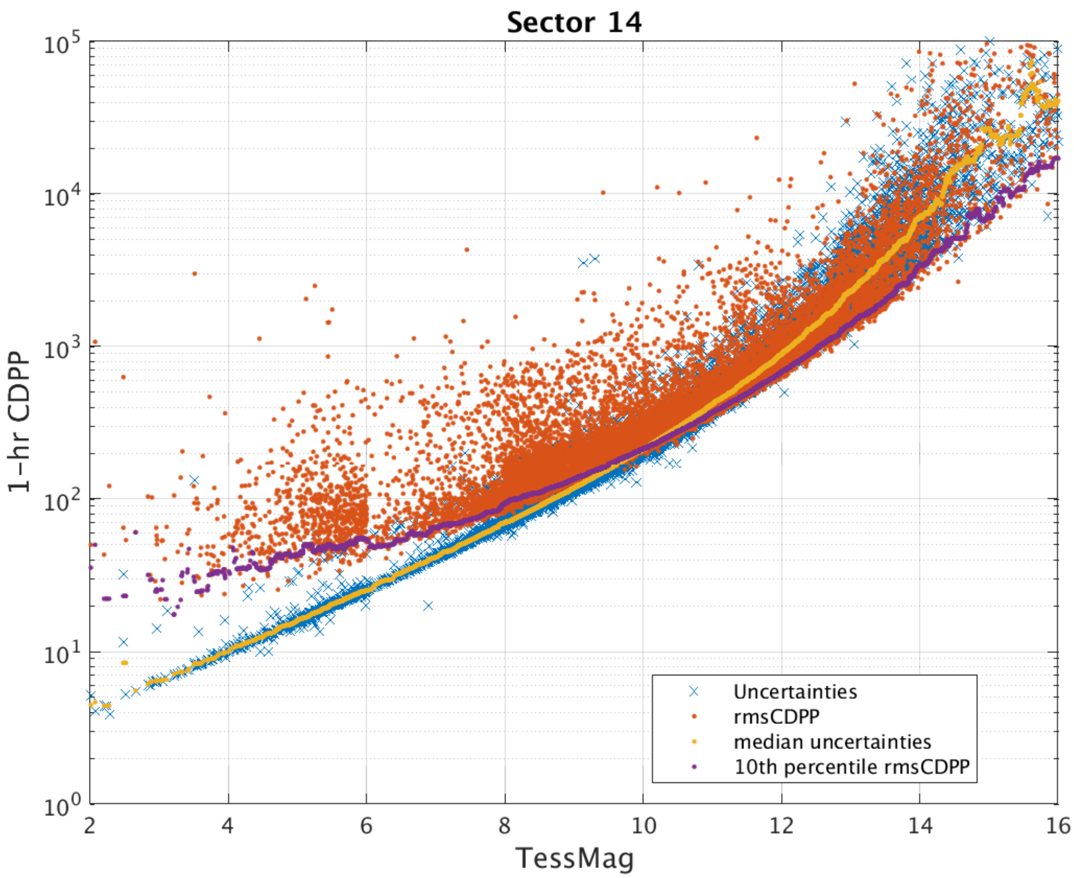

Figure 6: 1-hour CDPP. The red points are the RMS CDPP measurements for the 19993 light curves from Sector 14 plotted as a function of TESS magnitude. The blue x's are the uncertainties, scaled to 1-hour timescale. The purple curve is a moving 10th percentile of the RMS CDPP measurements, and the gold curve is a moving median of the 1-hr uncertainties.

camera FOV—that may appear one or two at a time (fireflies) or in large groups (fireworks). See the TESS Instrument Handbook for a more complete description.

4 Pipeline Performance and Results

4.1 Light Curves and Photometric Precision

Figure 5 gives the PDC goodness metrics for residual correlation and introduced noise on a scale between 0 (bad) and 1 (good). The performance of PDC is very good and generally uniform over most of the field of view. Figure 6 shows the achieved Combined Differential Photometric Precision (CDPP) at 1-hour timescales for all targets.

Table 2: Sector Fireflies and Fireworks

FFI Start	FFI End	Cameras	Description
2019202015929	2019202015929	2, 3, 4	Firefly
2019213222929	2019213225929	2	Firefly

4.2 Transit Search and Data Validation

In Sector 14, the light curves of 19993 targets were subjected to the transit search in TPS. Of these, Threshold Crossing Events (TCEs) at the $7.1\,\sigma$ level were generated for 946 targets.

In Sector 14, a new procedure for conducting the transit search was implemented. TPS utilizes "deemphasis weights" to decrease the weighted contribution of individual cadences to the single event statistics used to detect TCEs. Previously, these deemphasis weights were generated with smooth analytic functions to handle gaps and edge effects in the light curves. In Sector 14, the improved pipeline combines analytic deemphasis weights with data-driven deemphasis weights that suppress problematic epochs.

First, the top panel of Figure 7 was generated from an initial run of TPS, and was used to identify cadences with a 3σ excess of TCEs (red peaks in the top panel of Figure 7). These cadences were then assigned an additional deemphasis weight proportional to the magnitude of the TCE excess. Finally, TPS was rerun on all targets with both the original and these new deemphasis weights. Because epochs with excess TCEs mark instrumental or systematic issues (usually related to pointing jitter or scattered light and glints), this procedure removes many false positives and therefore increases the likelihood of detecting true transits. The final set of TCEs and the results reported here are based on the second run of TPS. The values of the adopted deemphasis weights are provided in the DV timeseries data products for targets with TCEs.

The bottom panel of Figure 7 shows the number of TCEs at a given cadence that exhibit a transit signal in the final set—this figure is much flatter than previous sectors because of the procedure described above. The top panel of Figure 8 shows the distribution of orbital periods for the final set of TCEs found in Sector 14.

The vertical histogram in the right panel of Figure 8 shows the distribution of transit depths derived from limb-darkened transiting planet model fits for TCEs. The model transit depths range down to the order of 100 ppm, but the bulk of the transit depths are considerably larger.

A search for additional TCEs in potential multiple planet systems was conducted in DV through calls to TPS. A total of 1427 TCEs were ultimately identified in the SPOC pipeline on 946 unique target stars. Table 3 provides a breakdown of the number of TCEs by target. Note that targets with large numbers of TCEs are likely to include false positives.

Finally, for some TCEs in the plane of the Galaxy, the difference images in the DV reports are completely covered by the large number of faint stars in TIC 8. For future data releases, the number and magnitude of stars shown in the difference images may be limited in order to clearly show the pixel data.

Table 3: Sector 14 TCE Numbers

Number of TCEs	Number of Targets	Total TCEs
1	564	564
2	309	618
3	53	159
4	15	60
5	4	20
6	1	6
–	946	1427

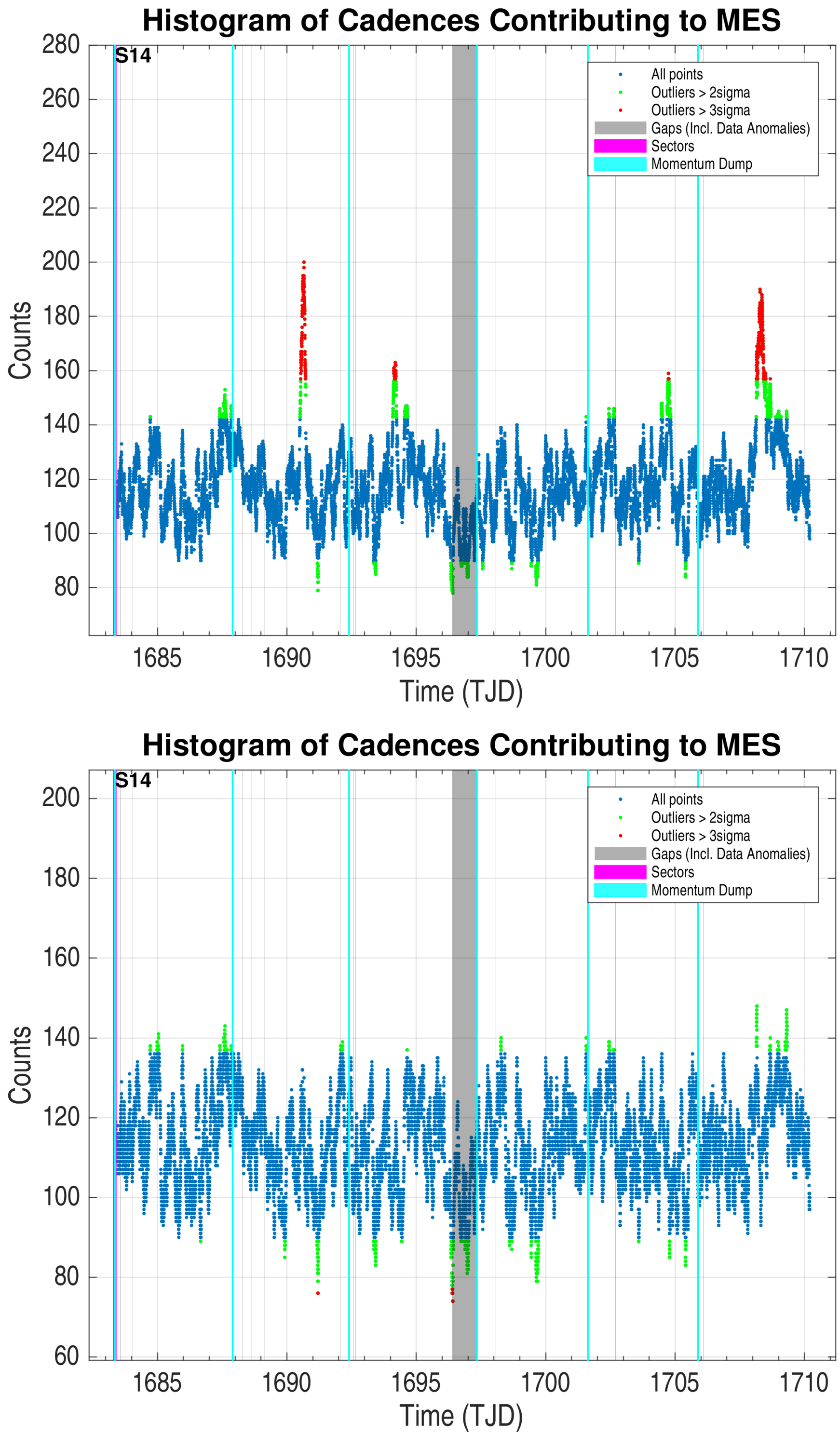

Figure 7: Top panel: Number of TCEs at a given cadence exhibiting a transit signal, based on an initial run of TPS. Any isolated peaks are caused by single events that result in spurious TCEs. These peaks were used to define deemphasis weights that suppress the contribution of problematic epochs to the transit detection statistics in a second iteration of TPS. Bottom panel: Results from the second run of TPS.

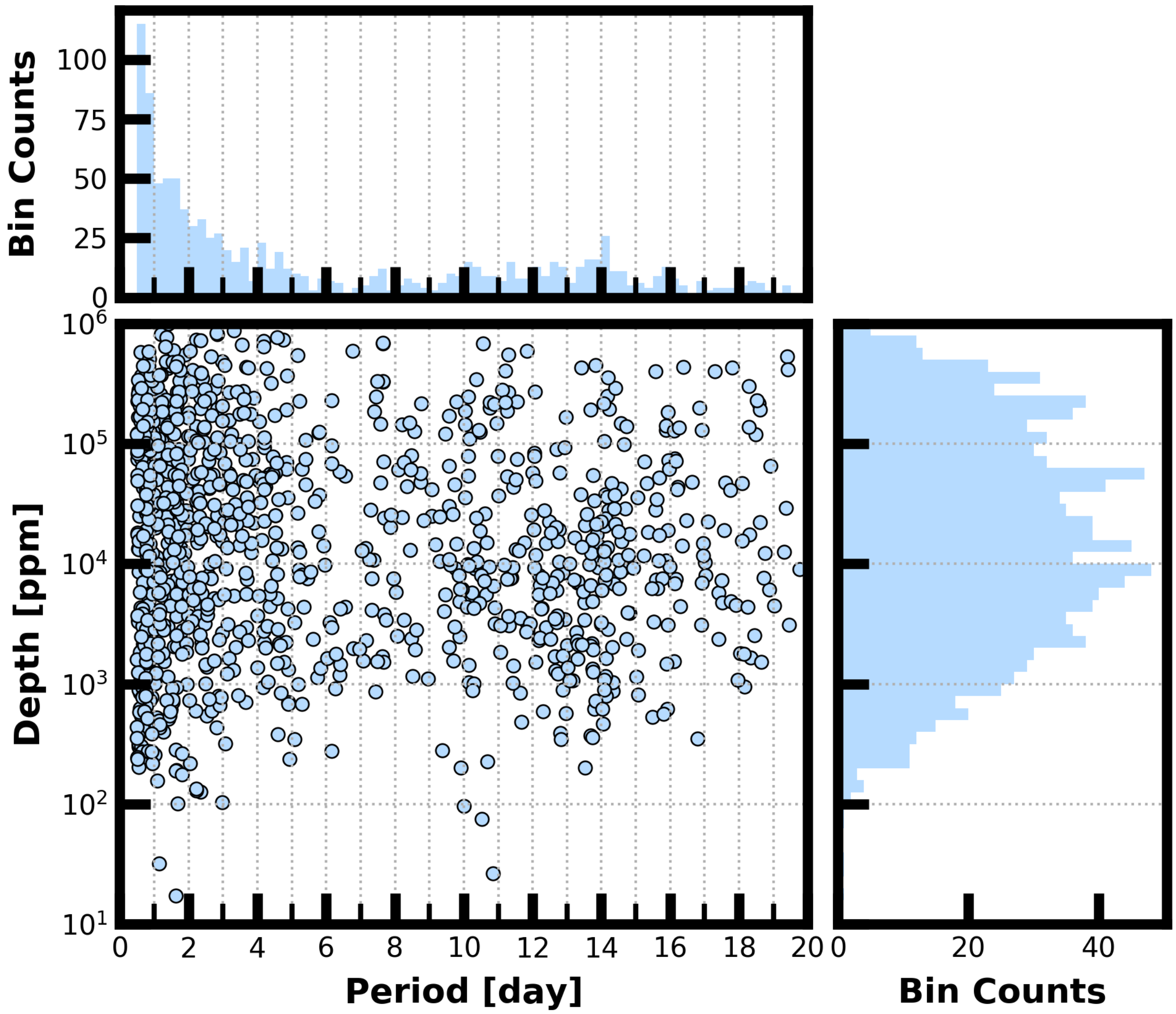

Figure 8: Lower Left Panel: Transit depth as a function of orbital period for the 1427 TCEs identified for the Sector 14 search. For enhanced visibility of long period detections, TCEs with orbital period <0.5 days are not shown. Reported depth comes from the DV limb darkened transit fit depth when available, and the DV trapezoid model fit depth when not available. Top Panel: Orbital period distribution of the TCEs shown in the lower left panel. Right Panel: Transit depth distribution for the TCEs shown in the lower left panel.

References

Jenkins, J. M. 2017, Kepler Data Processing Handbook: Overview of the Science Operations Center, Tech. rep., NASA Ames Research Center

Jenkins, J. M., Twicken, J. D., McCauliff, S., et al. 2016, in Proc. SPIE, Vol. 9913, Software and Cyberinfrastructure for Astronomy IV, 99133E

Li, J., Tenenbaum, P., Twicken, J. D., et al. 2019, *PASP*, 131, 024506

Stassun, K. G., Oelkers, R. J., Paegert, M., et al. 2019, *Astron. J.*, 158, 138

Twicken, J. D., Catanzarite, J. H., Clarke, B. D., et al. 2018, *PASP*, 130, 064502

Vanderspek, R., Doty, J., Fausnaugh, M., et al. 2018, TESS Instrument Handbook, Tech. rep., Kavli Institute for Astrophysics and Space Science, Massachusetts Institute of Technology

Acronyms and Abbreviation List

BTJD Barycentric-corrected TESS Julian Date

CAL Calibration Pipeline Module

CBV Cotrending Basis Vector

CCD Charge Coupled Device

CDPP Combined Differential Photometric Precision

COA Compute Optimal Aperture Pipeline Module

CSCI Computer Software Configuration Item

CTE Charge Transfer Efficiency

Dec Declination

DR Data Release

DV Data Validation Pipeline Module

DVA Differential Velocity Aberration

FFI Full Frame Image

FIN FFI Index Number

FITS Flexible Image Transport System

FOV Field of View

FPG Focal Plane Geometry model

KDPH Kepler Data Processing Handbook

KIH Kepler Instrument Handbook

KOI Kepler Object of Interest

MAD Median Absolute Deviation

MAP Maximum A Posteriori

MAST Mikulski Archive for Space Telescopes

MES Multiple Event Statistic

NAS NASA Advanced Supercomputing Division

PA Photometric Analysis Pipeline Module

PDC Pre-Search Data Conditioning Pipeline Module

PDC-MAP Pre-Search Data Conditioning Maximum A Posteriori algorithm

PDC-msMAP Pre-Search Data Conditioning Multiscale Maximum A Posteriori algorithm

PDF Portable Document Format

POC Payload Operations Center

POU Propagation of Uncertainties

ppm Parts-per-million

PRF Pixel Response Function

RA Right Ascension

RMS Root Mean Square

SAP Simple Aperture Photometry

SDPDD Science Data Product Description Document

SNR Signal-to-Noise Ratio

SPOC Science Processing Operations Center

SVD Singular Value Decomposition

TCE Threshold Crossing Event

TESS Transiting Exoplanet Survey Satellite

TIC TESS Input Catalog

TIH TESS Instrument Handbook

TJD TESS Julian Date

TOI TESS Object of Interest

TPS Transiting Planet Search Pipeline Module

UTC Coordinated Universal Time

XML Extensible Markup Language